Terahertz intersubband absorption and conduction band alignment in *n*-type Si/SiGe multiple quantum wells

G. Ciasca, M. De Seta, G. Capellini, and F. Evangelisti
Dipartimento di Fisica, Università di Roma Tre, via Vasca Navale 84, I-00146 Roma, Italy

M. Ortolani
Istituto di Fotonica e Nanotecnologie, IFN-CNR, Via Cineto Romano 42, I-00156 Roma, Italy

M. Virgilio and G. Grosso
Dipartimento di Fisica "E. Fermi" and CNR-NEST-INFM, Università di Pisa, Largo Pontecorvo 3, I-56127 Pisa, Italy

A. Nucara and P. Calvani
Dipartimento di Fisica and CNR-INFM Coherentia, Università di Roma La Sapienza, Piazzale A. Moro 2, I-00185 Roma, Italy
(Received 7 November 2008; published 3 February 2009)

Absorption due to conduction intersubband transitions is studied in *n*-type s-Si/SiGe multiquantum wells (MQW) of different well widths and barrier composition grown by UHV-chemical vapor deposition (CVD). The measured intersubband transition energies are compared with the theoretical results of a tight-binding model which provides the electronic band structure of the complete MQW system throughout the whole Brillouin zone. Our findings demonstrate both the high quality of the CVD grown MQWs and the effectiveness of the adopted tight-binding model in describing band profiles and electronic structures of SiGe multilayer systems. In particular we have evaluated the conduction band offsets in the investigated structures.

DOI: 10.1103/PhysRevB.79.085302 PACS number(s): 78.67.De, 73.21.Fg, 68.65.Fg, 81.15.Gh

I. INTRODUCTION

The successful fabrication of GaAs/AlGaAs-based quantum cascade lasers (QCL) (Refs. 1 and 2) has stimulated an intense research effort toward the performance improvement of sources emitting in the terahertz range of the electromagnetic spectrum. However, owing to intrinsic limitations of GaAs/GaAlAs sources,[3] novel heterostructures with more promising properties have been recently investigated. Among them, the SiGe heterostructure is one of the more interesting since it is a nonpolar system and potentially operable at high temperature and in a wide frequency range. Moreover, the fabrication of a Si-based QCL source would enable a photonic platform monolithically integrated in the standard CMOS technology.

So far, experimental investigations for developing a SiGe-based QCL have been focused on *p*-type structures grown on relaxed SiGe(001) substrates having a Ge composition in the $x=0.2-0.4$ range,[4–6] exploiting the intense confining potentials in the valence band. Moreover, holes have a smaller effective mass in the tunneling direction as compared to Δ_2 valley electrons, thus allowing for the use of thicker, and easier-to-grow, barriers for carrier injection. On the other hand, coupling among different hole subbands has been the most serious obstacle for the realization of a silicon-germanium quantum cascade laser.

Exploiting conduction band transitions would render the fabrication of a Si/SiGe QCL conceptually simpler, albeit challenging from the practical point of view. A conduction band offset large enough to obtain intersubband transitions in the terahertz energy range has been theoretically predicted[7–9] for in-plane tensile strained Si grown on relaxed $Si_{1-y}Ge_y$ layers with $0.2<y<0.5$. Very recently, terahertz emission from *n*-type Si/SiGe quantum cascade (QC) heterostructures in this compositional range was theoretically investigated and positive gain predicted.[10] From the experimental side, an exhaustive characterization of conduction intersubband transitions is still lacking. To the best of our knowledge, only two papers have dealt with this problem. Hertle *et al.*[11] have measured absorption peaks related to intersubband transitions in two multiple Si-quantum wells samples of different widths confined by $Si_{0.5}Ge_{0.5}$ barriers grown by molecular-beam epitaxy (MBE) on a $Si_{0.7}Ge_{0.3}$ virtual substrate. Fujita *et al.*[12] reported intersubband transitions in MBE-grown superlattices with $Si/Si_{0.4}Ge_{0.6}$ unit cells of different widths. Intersubband transitions on samples grown by CVD have not been reported as yet.

In order to fabricate a QCL structure, a sequence of Si/SiGe multilayers must be grown pseudomorphically on a planar $Si_{1-y}Ge_y$ substrate whose composition is chosen to ensure the wanted strain distribution in the active part of the device and to avoid plastic relaxation. Relaxed virtual substrate (VS) of a given Ge composition can be obtained by composition-graded SiGe buffer layers grown on a Si(001) substrate followed by a thick SiGe buffer layer of the desired composition.[8,13] Recently, alternative to graded VSs, SiGe on insulator (SGOI) and tensile strained silicon on insulator (sSOI) have become available.[14] These substrates offer several advantages with respect to SiGe VSs. They are dislocation free, allow very good strain uniformity and control, and have surface roughness values more than 1 order of magnitude lower than that typically measured on the cross-hatched VS surfaces.[15,16] These features are of great interest for the realization of QCLs, where nanometric control of compositions, strain, and thicknesses is required. Furthermore, the presence of a buried oxide layer of appropriate thickness

reduces current leakages and shunts in optoelectronic devices and may be exploited for the fabrication of integrated optical cavities.

In this work we have investigated *n*-type s-Si/SiGe multiquantum well (MQW) structures grown by means of chemical vapor deposition on SGOI and sSOI substrates as well as on graded VS. By measuring the absorption peaks due to intersubband transitions between the s-Si confined fundamental (E_0) and the first-excited (E_1) levels, we demonstrate a significant conduction band offset in these structures. In order to quantify this band offset we exploit a tight-binding (TB) model which provides the electronic band structure of the complete MQW systems throughout the whole Brillouin zone. The observed features and the agreement between theoretical and experimental data demonstrate both the high quality of the CVD grown MQW and the effectiveness of the adopted tight-binding model for evaluating band profile and electronic structures. This is a particularly important result since, for the MQW here considered, the conduction band lineup has been debated without a general consensus due to the requirement to precisely assign the position of the Δ_2 and Δ_4 conduction valley energies in the presence of alloying and strain effects.[7–9]

The paper is organized as follows: in Sec. II, we describe the investigated systems reporting details on the sample growth and experimental methods adopted; the measured intersubband transmission spectra are reported in Sec. III A; in Sec. III B we present the tight-binding method adopted to describe the electronic states of the investigated MQW samples, compare the calculated transition energies with the measured absorption peaks, and evaluate conduction band offset values for the s-Si/$Si_{1-x}Ge_x$ interfaces here investigated; our conclusions are given in Sec. IV.

II. SAMPLE GROWTH AND EXPERIMENTAL METHOD

The Si and SiGe layers were grown by ultrahigh vacuum chemical vapor deposition technique from high-purity silane and germane. The *n*-type doping was obtained by adding to growth gases phosphine diluted in molecular hydrogen.

The multiquantum well structures (MQWS) investigated were grown on three different types of substrates: namely VS, SGOI, and sSOI.

The VSs were obtained by depositing on Si (001) wafers a 2.8-μm-thick linearly graded SiGe buffer layer with final Ge fractional content x equal to 20%, followed by a 2.0-μm-thick $Si_{0.80}Ge_{0.20}$ layer.

The SGOI and sSOI substrates were cut from 8 in. substrates fabricated by means of the Smart-Cut™ technique by SOITEC.[17] Their structures consist, respectively, of a 23-nm-thick $Si_{0.8}Ge_{0.2}$ layer and of a 60-nm-thick strained Si layer bonded on a 150-nm-thick thermal oxide. The strained Si layer has a 0.8% tensile strain, corresponding to strained Si pseudomorphic to relaxed $Si_{0.80}Ge_{0.20}$.

Since the quality of the heterostructures critically depends on the structure and cleanliness of the substrate surface, a cleaning procedure of the sSOI and SGOI substrates suitable for the epitaxial growth was implemented. After preliminary ultrasonic bath in isopropyl alcohol, the substrates underwent an *ex situ* wet chemical cleaning in a $H_2O_2:H_2SO_4$ 1:2 solution for 3 min, followed by a dip in 1% diluted hydrofluoric acid for 80 s and, finally, were immersed in $H_2O_2:H_2SO_4$ 1:2 solution for 6 min. The surface cleaning was completed by an *in situ* thermal heating up to 850 °C in H_2 atmosphere for desorbing the residual O and C present on the surface. *In situ* x-ray photoemission spectroscopy measurements indicate that this cleaning procedure preserves the composition of the SGOI SiGe layer. Raman and x-ray diffraction measurements evidence that the thermal treatment does not alter the strain status and the composition the sSOI and SGOI substrates.[18]

Prior to the MQWs growth, a 100-nm-thick $Si_{0.80}Ge_{0.20}$ buffer layer was deposited at $T=850$ °C on the clean surface. The typical surface rms roughness of the SiGe buffer layer, as measured by atomic force microscopy (AFM), was ≤ 0.5 nm. This value is significantly lower than that found on graded SiGe virtual substrates. In the latter case the cross-hatch pattern dominates the surface morphology, and the typical surface rms roughness is ~ 6 nm.

Two series of modulation doped MQWs were grown at $T=700$ °C. In the A series the MQWs are made up of variable thickness s-Si wells and relaxed *n*-doped $Si_{0.80}Ge_{0.20}$ barriers while in the B series they are made up of variable thickness s-Si wells and compressively strained *n*-doped $Si_{0.64}Ge_{0.36}$ barrier layers. The 10 nm central regions of each barrier have been doped with phosphorus. Finally a relaxed $Si_{0.80}Ge_{0.20}$ cap layer of 100 nm was grown to complete the structure. The characteristics of all the samples investigated in this study are summarized in Table I.

The carrier concentration per well of the sample D were determined by Hall measurements and resulted to be $n_{2D}=3\times10^{12}$ cm^{-2}. We also found that the presence of 5-nm-thick spacer layers between the doped part of the barriers and the wells (samples E, F, I, and L) reduces the carrier concentration by 1/3.

Thickness and morphology of the different layers have been determined by means of a 160 keV transmission electron microscope (TEM). A typical TEM image is reported in the top right panel of Fig. 1. The data showed the regularity of the layers and the abruptness of the interfaces (within 0.5 nm). The absence of any dislocation feature and the analysis of Raman measurements (to be published) suggest that strain relaxation did not occur in MQWs even when the structures were not strain compensated.

The infrared transmission spectra of the samples were measured using a rapid-scan Michelson interferometer. Since the Si mass tensor is diagonal in the reference system of the growth direction, intersubband transitions are only allowed for incidence radiation with electric field in the growth direction, i.e., they are forbidden for normal-incidence radiation.[19] Therefore, in order to observe intersubband absorption, the samples were cut in a waveguide shape with lateral facets at 45°, as depicted in the sketch of Fig. 1. The lateral facets as well as the back side were optically polished and the top (growth) side was coated with a 5-nm-thick Cr layer followed by an 80-nm-thick Au metallization. The waveguide length of the analyzed samples was between 3 and 5 mm and the total samples thickness was 0.7 mm. As a consequence the number of reflections occurring inside the waveguide varies between 3 and 5 (the oxide layer is too thin

TABLE I. Composition and structural characteristics of the studied MQW samples, $E_1 \rightarrow E_0$ intersubband transition energies, and absorption coefficient α_M as measured from the far infrared transmission spectra ($\Delta\alpha/\alpha \mp 15\%$). The central 10 nm of B-F and H-L sample barriers have been doped with a fixed donor concentration. In samples A and G the donor concentration was reduced by 1/3. The transmission spectra of sample A were acquired at 70 K.

Sample/ sub	Number of QW	Well width (nm)	Barrier Ge content	Barrier thickness (nm)	E_1-E_0 (meV)	FWHM (meV)	α_M (cm^{-1})
A/VS	10	3.9 ± 0.3	20%	10	57 ± 2		
B/SSOI	5	5.0 ± 0.2	20%	10	40.3 ± 0.6	6.3	3200
C/SGOI	8	6.0 ± 0.2	20%	10	32.1 ± 0.6	6.8	3500
D/SSOI	5	6.0 ± 0.2	20%	10	33.1 ± 0.6	6.8	4500
E/VS	10	5.5 ± 0.2	20%	20	37.2 ± 0.6	6	1800
F/VS	8	7.3 ± 0.3	20%	20	24.7 ± 0.6	5.8	2900
G/VS	10	3.5 ± 0.3	36%	10	70.8 ± 0.6	7	4100
H/VS	10	4.9 ± 0.3	36%	10	46.1 ± 0.6	6.6	6000
I/VS	10	4.9 ± 0.3	36%	20	47.1 ± 0.6	6.7	2900
L/VS	8	6.6 ± 0.3	36%	20	29.6 ± 0.6	6.4	3400

to produce total reflection at these wavelengths). The samples were then sandwiched between two copper plates and mounted in a He-flow optical cryostat. In this way the portion of the incoming beam not entering the waveguide was blocked by the copper plates. The waveguide propagation direction was set at 45° with the probe beam direction, i.e., at quasinormal angle of incidence, in order to minimize

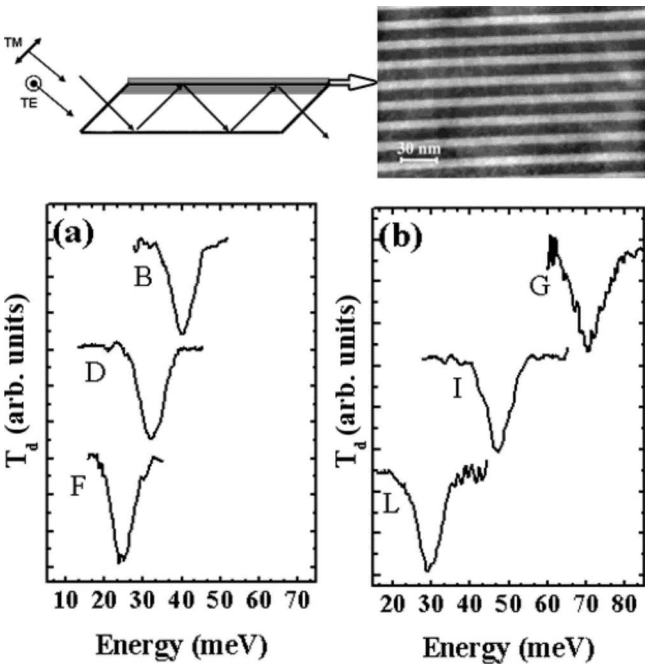

FIG. 1. Top panels: (left) sketch of the sample geometry used in the absorption measurements together with a TEM image of a typical MQW structure. Bottom panels: measured T_M/T_E transmission ratio T_d versus incident photon energy at 15 K for (a) MQWs between relaxed $Si_{0.80}Ge_{0.20}$ barriers and (b) MQWs between strained $Si_{0.64}Ge_{0.36}$ barriers. The waveguide geometry and the T_M and T_E light polarization directions are shown in the inset.

polarization-dependent reflectivity losses at the entrance facet. The lateral facet orientation is such that the output beam, after several reflections inside the waveguide, is parallel to the probe beam and is then directed to the detector. By using a 4.2 K Si bolometer in the far-infrared range (photon energies of 15–60 meV) and a 77 K broadband HgCdTe detector in the midinfrared range (55–300 meV), sample transmission spectra with values down to 0.01 could be measured with a conventional blackbody source.

The beam entering the waveguide was linearly polarized with a wire-grid polarizer. We measured for each sample both the transmitted spectra $T_E(\nu)$ with the electric field polarized orthogonal to the growth axis and $T_M(\nu)$, which has a component along the growth axis.

In the vicinity of the Au-metallization layer where the active MQWs region is located, the component orthogonal to the growth axis is strongly suppressed by phase matching effects, so that absorption features in $T_M(\nu)$ are only produced by dipole moments parallel to the growth axis (such as in intersubband transitions).

To account for the linear dichroic properties of the apparatus, $T_E(\nu)$ and $T_M(\nu)$ have been normalized using the $S_E^0(\nu)$ and $S_M^0(\nu)$ transmission spectra measured without a sample loaded in the cryostat.

III. RESULTS AND DISCUSSION

A. Experimental results

In Fig. 1 we show typical linear dichroic transmission spectra ($T_d = T_M/T_E$) of some of our samples in the energy range where intersubband transitions are expected. While several absorption lines are present in T_M and T_E spectra, the dichroic spectra are characterized by the presence of a single pronounced transmission dip, originating in the T_M mode, whose position shifts to higher energies upon decreasing the well width and/or increasing the Ge concentration in the bar-

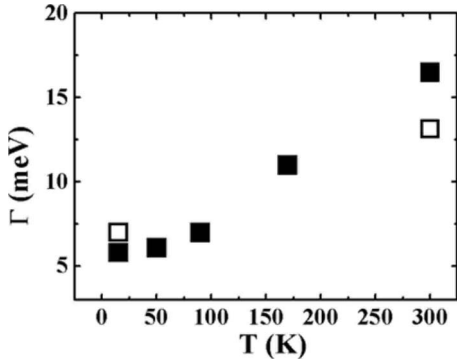

FIG. 2. FWHM Γ as a function of temperature of samples F (solid squares) and G (open).

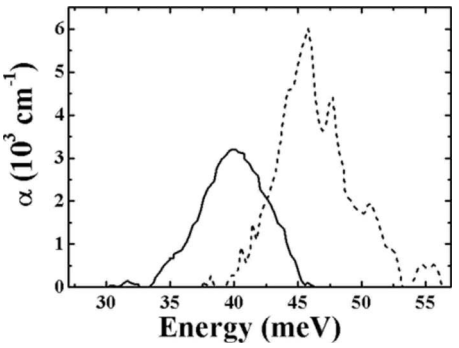

FIG. 3. Absorption coefficient of samples B (solid line) and H (dashed line) versus photon energy.

riers (see Table I). Depending on the number of periods in the MQW structure and on the waveguide length, the transmission reduction in the spectra is in the range 10%–50%. As will be argued in the following, we identify this feature as due to the $E_0 \rightarrow E_1$ intersubband transition.

The measured full width at half maximum (FWHM) at 15 K is $\Gamma = 6-7$ meV for all the investigated samples (see Table I). Similar values were observed in the transmission spectra measured at 8 K on MBE grown samples.[11] As shown in Fig. 2, where the temperature dependence of the FWHM of the samples F and G is reported, the dip width remains almost constant up to $T = 50$ K and then increases, reaching a value $\Gamma \sim 13-16$ meV at 300 K.

Single particle calculations show that the absorption-line width in narrow-well structures, i.e., wells corresponding to subband spacing >10 meV, is dominated by interface roughness scattering at low temperature with the phonon-scattering contribution becoming relevant only at higher temperature.[20–22] Although we found Γ values of the same order of magnitude of those obtained theoretically, the calculations predict a stronger dependence of Γ on the well width. In particular, increased Γ values are expected for $W < 6$ nm. This suggests that other effects, not included in these calculations, may contribute to the absorption-line shape. For instance, vertical correlation between adjacent interfaces, many-body and band nonparabolicity effects have been reported to influence Γ.[23–25]

The absorption coefficient $\alpha(E)$ was estimated from the relationship

$$e^{-\alpha(E)(N_w p L/\cos\phi)} = \frac{T_M}{T_E},$$

where N_w is the number of QW comprised in the structure, p is the number of reflections of the infrared radiation propagating in the waveguide, L the width of a barrier-QW unit, and $\varphi = 45°$ the angle between the beam and the growth directions.

As an example, we display in Fig. 3 the absorption coefficient $\alpha(E)$ for the samples B (solid line) and H (dashed, see Table I) having the same QW thickness (5 nm) and barrier thickness (10 nm) but different barrier composition ($x = 0.2$ and $x = 0.36$, respectively).

In Table I we report the value at the maximum α_M of the absorption coefficient of all the samples here investigated. As expected the absorption coefficient increases with the carrier density: samples without spacer layers in the barrier have increased α_M (compare α_M values of samples C–D and samples H–I). The observed larger values of α_M for samples with $Si_{0.64}Ge_{0.36}$ barriers can be related to the increased barrier height. As a matter of fact an increased barrier height favors the charge transfer from the donor states to the well E_0 subband, i.e., the carrier density is expected to be higher in a s-Si well sandwiched between $Si_{0.64}Ge_{0.36}$ barriers.

The measured integrated absorption $\int \alpha(E) dE$ of our samples ranges from 1×10^4 to 4×10^4 cm^{-1} meV in good agreement with the theoretical results of Ref. 19 for an sSi/SiGe system having a carrier concentration of $\sim 10^{12}$ cm^{-2}.

B. Numerical calculations

In this section we report theoretical results obtained by means of a tight-binding model for the electronic states of the MQW structures considered above.

The tight-binding model has proven to be an accurate theoretical tool for the description of SiGe optical devices.[19,26–28] In fact this atomistic approach allows taking into account the geometric details of the whole structure, the chemical composition of the substrate and of the deposited materials, the strain within each layer and the spin-orbit coupling. The method provides the energy-band structure over the whole Brillouin zone, the spatial and orbital compositions of the states and the optical matrix elements for inter-[26,28] and intraband[19,27] optical transitions. Furthermore, band alignments,[9] band folding, and intervalley interactions[27] have been also described within the same formalism.

The tight-binding Hamiltonian here adopted is expressed on a $sp^3d^5s^*$ atomiclike basis set, considering first-neighbor interactions and spin-orbit coupling. The on-site and hopping Hamiltonian matrix elements for Si and Ge crystals are taken from the semiempirical parameterizations derived in Ref. 29 to describe bulk electronic states at low temperature. Since Si and Ge are miscible in the whole composition range, alloying is modeled in the virtual-crystal approximation. A recent discussion of such approximation in the TB framework can be found in Ref. 30. Effects of strain are accounted for by suitable scaling laws for the hopping parameters[29] after

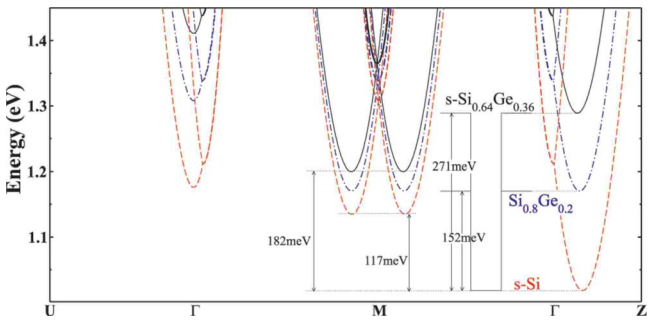

FIG. 4. (Color online) Conduction electronic band structures of the *bulk* crystals composing the relaxed $Si_{0.80}Ge_{0.20}$ (blue, dotted-dashed line), the strained $Si_{0.64}Ge_{0.36}$ (black, solid line) barrier material, and the s-Si well (red, dashed line). The points U, M, and Z of the adopted tetragonal BZ correspond to the L, $X_{\|}$, and $X_{\perp}$ points of the octahedral BZ, respectively. Parallel and orthogonal directions are referred to the growth plane. The quoted value of 117 meV represents the energy difference between conduction minima along the $\Gamma-M(\Delta_4)$ and $\Gamma-Z(\Delta_2)$ lines in s-Si. The sketched conduction band profiles represent the band edges at the minima along the $\Gamma-Z$ line.

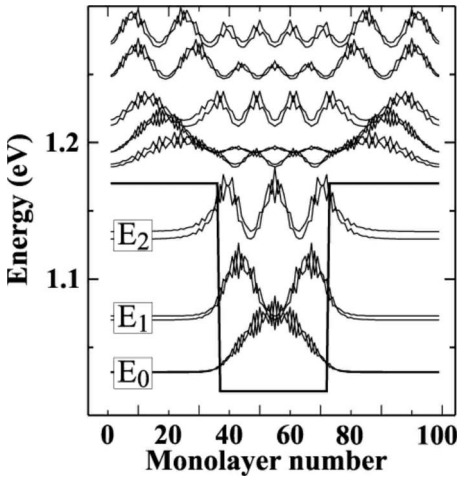

FIG. 5. Square modulus of the wave functions for the near gap conduction electronic states of sample B. The conduction band-edge profile is also reported. Layers from 37 to 72 correspond to the s-Si QW region. Continuum states above the barrier edge are also shown.

evaluation of the equilibrium positions of the ions by means of elasticity theory as discussed in Ref. 31. Bands alignment along the growth direction is inserted in the model adding a constant diagonal term in each homogeneous region of the system and setting as reference energy the topmost valence band in the buffer material. These values are chosen so to reproduce the valence-band offsets evaluated in Ref. 32. Discontinuities in the conduction band-edge profiles at the interfaces between barrier and well materials are then obtained from the calculation of the bulk band structure of the two materials as shown in Fig. 4 for barrier Ge-concentration equal to 0.20 and 0.36. For these two chosen Ge concentrations, the conduction band offsets ΔE_c (defined as the difference between the lowest conduction band energy in adjacent layers) at the interface with the s-Si region are 152 and 182 meV and the energy differences $\Delta E_c^{\Delta_2}$ between the conduction minima along the Δ_2 line are 152 and 271 meV, respectively.

In Fig. 5 we report the tight-binding results for the modulus square of the near gap wave functions calculated at the bottom of the conduction band of sample B ($x=0.20$). These states are found localized in the s-Si region as evidenced by the band-edge profile also shown in the figure. The square-well potential confines three subbands (E_0, E_1, E_2). For each of them, as well as for the higher energy states, we find the oscillating behavior and the fine doublet structure which is the typical signature of intervalley interaction.[27,33,34]

From the measured carrier densities we deduce that only the lowest (E_0) subband is populated at low temperature. Moreover, observing that the energy difference between the calculated E_0 and E_1 levels lies in the region where the measured absorption peaks are found, we conclude that these peaks are to be assigned to the $E_0 \rightarrow E_1$ transitions. In order to give further support to this claim, in Figs. 6(a) and 6(b) we compare the measured values of the $E_0 \rightarrow E_1$ transitions with the corresponding tight-binding values. We have also reported the value of the E_0-E_1 energy difference evaluated in the effective-mass approximation by means of both the infinite square-well model and the finite square-well model with barrier heights taken from the TB calculations (see Fig. 4) and using the measured effective masses.[35] We observe that the tight-binding model well reproduces the measured data which are underestimated by the finite QW model and overestimated by the infinite QW model, especially for thin QWs. The small difference ΔE between measured and calculated transition energies observed for relatively large QW widths can be attributed to depolarization effects. As a matter of fact, this effect, which causes the optical transition to occur at higher energy,[11,36] is expected to be more important for larger well width. A depolarization shift of about 2 meV, i.e., of the same magnitude of the observed ΔE, is expected for s-Si wells 70-nm-wide and carrier densities $\sim 1 \times 10^{12}$ cm^{-2}.

Finally, motivated by the poor information existing in the literature on the conduction band offsets (CBO) in SiGe sys-

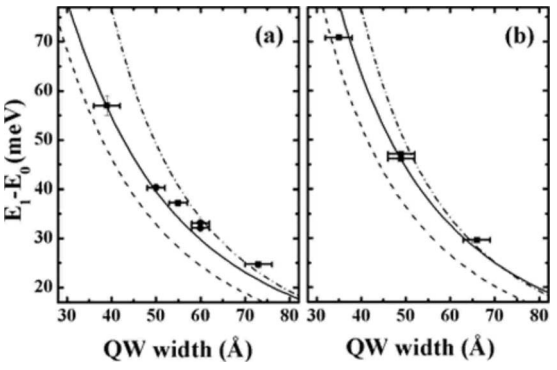

FIG. 6. Measured energies of the $E_0 \rightarrow E_1$ transitions as a function of the QW width (square symbols). The continuous lines represent the tight-binding results. Dotted-dashed and dashed lines represent the effective-mass results for the infinite and finite square-well models, respectively. (a) Refers to $Si_{0.80}Ge_{0.20}$ barriers and (b) to $Si_{0.64}Ge_{0.36}$ barriers, both grown on $Si_{0.80}Ge_{0.20}$ substrates.

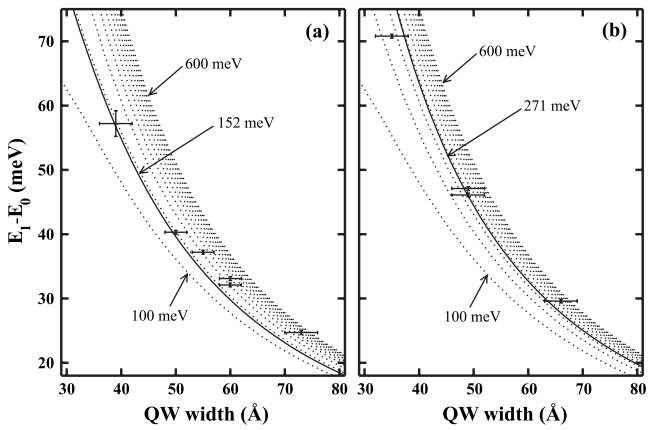

FIG. 7. $E_0 \rightarrow E_1$ transition energies as a function of the QW width calculated with the TB model for conduction band offset ranging in step of 50 from 100 meV (lowest dotted curves) to 600 meV (uppermost dotted curves). Continuous lines are obtained with the band alignment calculated as discussed in Sec. III B. Square symbols represent the measured $E_0 \rightarrow E_1$ transition energies. (a) refers to $Si_{0.80}Ge_{0.20}$ barriers and (b) to $Si_{0.64}Ge_{0.36}$ barriers, both grown on $Si_{0.80}Ge_{0.20}$ substrates.

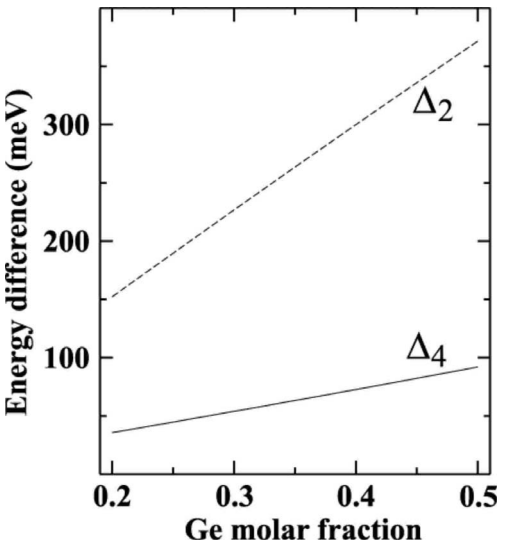

FIG. 8. Band offsets between compressively strained $Si_{1-x}Ge_x$ and tensile strained Si, epitaxially grown on a [001]-$Si_{0.80}Ge_{0.20}$ relaxed substrate, as a function of the Ge molar fraction x. Solid (dashed) line refers to the calculated energy difference $\Delta E_c^{\Delta_4}$ ($\Delta E_c^{\Delta_2}$) of conduction minima in the two layers along the Δ_4 (Δ_2) line.

tems, we have numerically investigated the sensitivity of the evaluated $E_0 \rightarrow E_1$ transition energies as a function of the height of the barriers. For this aim we have artificially varied the height of the QW by suitable modification of the diagonal terms of the system Hamiltonian so that different band alignments are obtained. The results for barrier heights in the range 100–600 meV are shown in Figs. 7(a) and 7(b) together with the measured transition energies. It is evident that the experimental intersubband transition energies are compatible only with well depth values close to the ones we have obtained from the calculations previously outlined $[\Delta E_c^{\Delta_2}=152(271)$ meV for barrier Ge-concentration equal to 0.20 (0.36)].

This fact supports the effectiveness of the TB model in predicting CBO values. For this reason we also report in Fig. 8 the conduction band offsets $\Delta E_c^{\Delta_2}$ and $\Delta E_c^{\Delta_4}$ along the Δ_2 and Δ_4 lines calculated for the s-Si/s-$Si_{1-x}Ge_x$ interface under the strain conditions imposed by a relaxed $Si_{0.80}Ge_{0.20}$ substrate, as a function of the Ge molar fraction in the $x=[0.20,0.50]$ range. Note that the Δ_4 minima in the compressively strained $Si_{1-x}Ge_x$ alloy have lower energy as compared to the Δ_2 ones, the opposite holding for tensile strained Si material. Nevertheless, for the chosen s-Si/s-$Si_{1-x}Ge_x$ interfaces, the energy minimum is always found in the Si region, both along the Δ_2 and the Δ_4 lines (see Fig. 4). From the above considerations it follows that $\Delta E_c^{\Delta_2}$ (which is the depth of the well sketched in Figs. 4 and 5) is larger than the corresponding $\Delta E_c^{\Delta_4}$ value, as shown in Fig. 8. As a matter of fact both alloying and strain cooperate to increase the energy difference of the conduction minima along the Δ_2 line while they have opposite sign along the Δ_4 line. Positive slope for the Δ_4 curve in Fig. 8 indicates that for the chosen Ge concentrations the alloy effect dominates.

IV. CONCLUSIONS

In summary, we have investigated intersubband transitions between the s-Si confined fundamental (E_0) and the first-excited (E_1) levels in CVD grown n-type $Si_{1-x}Ge_x$/s-Si/$Si_{1-x}Ge_x$ multiquantum wells of different well width, and barrier Ge concentration x equal to 0.2 and 0.36. The MQWs structures were grown on different substrates (SGOI and sSOI commercial substrates and graded SiGe VS) all having the in-plane lattice parameter of a relaxed $Si_{0.8}Ge_{0.2}$ alloy. We have measured transition energies in the 20–70 meV range depending on the well width and the barrier composition. The FWHM at 15 K was found to be ~6 meV almost independent of the well width, the barrier composition, and the substrate. Measured intersubband transition energies quite well compare with the energy difference between E_0 and E_1 levels calculated with a tight-binding model which provides the electronic band structure of the complete MQW systems throughout the whole Brillouin zone. We find for the conduction band offsets ΔE_c at the interface with the s-Si region the values 152 and 182 meV for barrier Ge-concentration equal to 0.20 and 0.36, respectively, while the corresponding energy differences between the conduction minima in the well and in the barrier along the Δ_2 line, $\Delta E_c^{\Delta_2}$, are 152 and 271 meV.

The good agreement between the measured intersubband transition energies and the TB results strongly supports the TB prediction of the CBO values here reported for general s-Si/s-$Si_{1-x}Ge_x$ heterointerfaces grown on a relaxed $Si_{0.80}Ge_{0.20}$ substrate.

The results here reported target the development of terahertz QC emitters based on intersubband transitions in the conduction band of Si/SiGe MQW heterostructures.

ACKNOWLEDGMENT

This work was partially supported by PRIN project "THz radiation generation in unipolar Si-Ge heterostructures."

[1] J. Faist, F. Capasso, D. L. Sivco, C. Sirtori, A. L. Hutchinson, and A. Y. Cho, Science **264**, 553 (1994).
[2] R. Kohler, A. Tredicucci, F. Beltram, H. E. Beere, E. H. Linfield, A. G. Davies, D. A. Ritchie, R. C. Iotti, and F. Rossi, Nature (London) **417**, 156 (2002).
[3] P. Harrison, D. Indjin, V. D. Jovanović, A. Mirčetić, Z. Ikonić, R. W. Kelsall, J. McTavish, I. Savić, N. Vukmirović, and V. Milanović, Phys. Status Solidi A **202**, 980 (2005)
[4] S. A. Lynch, R. Bates, D. J. Paul, D. J. Norris, A. G. Cullis, Z. Ikonic, R. W. Kelsall, P. Harrison, D. D. Arnone, and C. R. Pidgeon, Appl. Phys. Lett. **81**, 1543 (2002).
[5] I. Bormann, K. Brunner, S. Hackenbuchner, G. Abstreiter, S. Schmult, and W. Wegscheider, Appl. Phys. Lett. **80**, 2260 (2002).
[6] R. Bates, S. A. Lynch, D. J. Paul, Z. Ikonic, R. W. Kelsall, P. Harrison, S. L. Liew, D. J. Norris, and A. G. Cullis, Appl. Phys. Lett. **83**, 4092 (2003).
[7] M. M. Rieger and P. Vogl, Phys. Rev. B **48**, 14276 (1993).
[8] F. Schäffler, Semicond. Sci. Technol. **12**, 1515 (1997).
[9] M. Virgilio and G. Grosso, J. Phys.: Condens. Matter **18**, 1021 (2006).
[10] I. Lazic, Z. Ikonic, V. Milanovic, R. W. Kelsall, D. Indjin, and P. Harrison, J. Appl. Phys. **101**, 093703 (2007).
[11] H. Hertle, G. Schuberth, E. Gornik, G. Abstreiter, and F. Schäffler, Appl. Phys. Lett. **59**, 2977 (1991).
[12] K. Fujita, S. Fukatsu, Y. Shiraki, H. Yaguchi, and R. Ito, Appl. Phys. Lett. **61**, 210 (1992).
[13] D. J. Paul, Semicond. Sci. Technol. **19**, R75 (2004).
[14] B. Ghyselen, J. M. Hartmann, T. Ernst, C. Aulnette, B. Osternaud, Y. Bogumilowicz, A. Abbadie, P. Besson, O. Rayssac, A. Tiberj, N. Daval, I. Cayrefourq, F. Fournel, H. Moriceau, C. Di Nardo, F. Andrieu, V. Paillard, M. Cabie, L. Vincent, E. Snoeck, F. Cristiano, A. Rocher, A. Ponchet, A. Claverie, P. Boucaud, M. N. Semeria, D. Bensahel, B. Kernevez, and C. Mazure, Solid-State Electron. **48**, 1285 (2004).
[15] M. Myronov and Y. Shiraki, J. Cryst. Growth **301-302**, 315 (2007).
[16] K. Kutsukake, N. Usami, T. Ujihara, K. Fujiwara, G. Sazaki, and K. Nakajima, Appl. Phys. Lett. **85**, 1335 (2004).
[17] http://www.soitec.com/en/products/
[18] G. Capellini, G. Ciasca, M. De Seta, A. Notergiacomo, F. Evangelisti, and M. Nardone, J. Appl. Phys. (to be published).
[19] M. Virgilio and G. Grosso, Nanotechnology **18**, 075402 (2007).
[20] T. Unuma, M. Yoshita, T. Noda, H. Sakaki, and H. Akiyama, J. Appl. Phys. **93**, 1586 (2003).
[21] B. Mukhopadhyay and P. K. Basu, Phys. Status Solidi B **241**, 1859 (2004)
[22] A. Valavanis, Z. Ikonic, and R. W. Kelsall, Phys. Rev. B **77**, 075312 (2008).
[23] J. Li and C. Z. Ning, Phys. Rev. Lett. **91**, 097401 (2003).
[24] S. Tsujino, A. Borak, E. Muller, M. Scheinert, C. V. Falub, H. Sigg, D. Grutzmacher, M. Giovannini, and J. Faist, Appl. Phys. Lett. **86**, 062113 (2005).
[25] X. W. Mi, J. C. Cao, C. Zhang, and F. B. Meng, J. Appl. Phys. **98**, 103530 (2005).
[26] M. Virgilio and G. Grosso, Phys. Rev. B **77**, 165315 (2008).
[27] M. Virgilio and G. Grosso, Phys. Rev. B **75**, 235428 (2007).
[28] M. Bonfanti, E. Grilli, M. Guzzi, M. Virgilio, G. Grosso, D. Chrastina, G. Isella, H. von Kanel, and A. Neels, Phys. Rev. B **78**, 041407(R) (2008).
[29] J.-M. Jancu, R. Scholz, F. Beltram, and F. Bassani, Phys. Rev. B **57**, 6493(R) (1998).
[30] T. B. Boykin, N. Kharche, and G. Klimeck, J. Phys.: Condens. Matter **19**, 036203 (2007).
[31] J. Singh, *Electronic and Optoelectronic Properties of Semiconductor Structures* (Cambridge University Press, Cambridge, 2003).
[32] C. G. Van de Walle and R. M. Martin, Phys. Rev. B **34**, 5621 (1986).
[33] T. B. Boykin, G. Klimeck, M. A. Eriksson, M. Friesen, S. N. Coppersmith, P. von Allmen, F. Oyafuso, and S. Lee, Appl. Phys. Lett. **84**, 115 (2004).
[34] T. B. Boykin, G. Klimeck, M. Friesen, S. N. Coppersmith, P. von Allmen, F. Oyafuso, and S. Lee, Phys. Rev. B **70**, 165325 (2004).
[35] *Data in Science and Technology*, edited by O. Madelung, Landolt-Börnstein, New Series, Group III, Vol. 17, Pt. A (Springer-Verlag, Berlin, 1991).
[36] T. Ando, A. Fowler, and F. Stern, Rev. Mod. Phys. **54**, 437 (1982).